Streamer dynamics

M. C. Wang and E. E. Kunhardt
Weber Research Institute, Polytechnic University, Route 110, Farmingdale, New York 11735
(Received 16 January 1990)

An analysis of streamers is presented from the viewpoint of the interplay of the rate processes that contribute to their development. The space-time evolution of a streamer front is described by a sequence of stages that are identified by the dominant rate process determining the local properties of the front and the "turning point" where this process is overcome by others. Numerical and analytical results are used to determine these stages. From this analysis, the properties of positive (cathode-directed) and negative (anode-directed) streamers are elucidated, in particular, the dynamics that lead to the saturation of electron-density and electric-field enhancement. An expression is obtained that relates the dynamics of the positive and negative streamers associated with an initial space-charge distribution.

I. INTRODUCTION

In a number of situations, such as lightning and pulse breakdown of gases, the propagation of the ionized channel proceeds via an ionizing potential wave[1-5] (IPW). These are nonlinear waves that convert field energy in the region immediately ahead of the wave front into ionization and excitation energy of the gas and kinetic energy of all particles in the region behind the front. In general, the IPW arise from the interplay between the space-charge field, electron-impact ionization, gas photoionization, neutral gas heating, and the background conductivity of the region ahead of the front. There are various types of IPW (such as streamers and leaders) differentiated by the relative importance of the above effects in shaping their characteristics.[1-6]

In this paper we discuss the structure and dynamics of streamers.[7] They are a class of IPW in which the conductivity of the background gas ahead of the front is zero and neutral gas heating is not significant (the terminology of streamers is sometimes used to refer to all IPW, leading to confusion as to the importance of these effects). A considerable amount of experimental,[8-12] theoretical,[2-6] and numerical efforts[13-18] have been devoted to the understanding of the structure and propagation of streamers. Recent developments in diagnostic techniques have allowed a more quantitative probing of streamer structure and propagation.[10,11] The focus of most of these investigations has been on the speed of propagation and radius of the streamer channel. Because of the complexity of the equations describing streamer dynamics (either kinetic or fluid descriptions), analytical investigations have been restricted to one (longitudinal) spatial dimension (1D).[2-5] This simplification results in space-charge field distributions and consequently particle flows that may give an inaccurate picture of streamer dynamics.[15,17,18] Numerical simulations and experiments show that the radial flow of charge is important in determining the radial density profiles and, consequently, the field structure.[11] Thus, at least, a 2D analysis is necessary. Although kinetic models have been used,[13,18] the vast majority of the numerical simulations of streamers have used fluid equations to describe the evolution of the electron and ion densities.[14-17] The emphasis of these simulations has been primarily on determining the static structure of streamers, such as electron density and field distribution and the speed of propagation.

Our objective is to elucidate dynamical characteristics of streamers from the viewpoint of the interplay of the various rate processes that contribute to their development. Numerical and analytical results are used to provide a description of the evolution in space-time of the streamer front by identifying the dominant rate process that determines the local properties of the front and the "turning point" where this process is overcome by others. In this fashion, the structure of the streamer front is divided into (space-time) stages or domains associated with the local dominant process. From this analysis, the properties of cathode- and anode-directed streamers are determined, in particular, the dynamics that lead to the saturation of electron density and electric field enhancement due to the space charge. Moreover, the coupling between anode- and cathode-directed streamers propagating away from an initially isolated charge distribution has been determined.

The physical situation under investigation and its simulation model are presented in Sec. II. The results are discussed in Sec. III, and concluding remarks are given in Sec. IV.

II. FORMULATION OF THE PROBLEM AND ITS SIMULATION MODEL

A. Physical problem and basic equations

The physical problem investigated can be described as follows. Consider two infinite-parallel-plate electrodes separated by a distance d with a gas, at a density N, filling the interelectrode space. Equal distributions of electrons and ions are initiated in the middle of the space, and simultaneously, a voltage is applied to the electrodes, creating a uniform field $\mathbf{E}_a$ along the axial direction $\mathbf{a}_z$.

The initial charged-particle densities are chosen to be small enough that space-charge effects are initially insignificant (that is, the magnitude of the space-charge field is well below E_a).

The space-time evolution of the electron and ion densities is determined from the continuity equations;[17] namely, for electrons,

$$\partial_t n_e = -\nabla\cdot(n_e \mathbf{v}_e) + (\alpha-\eta) n_e |\mathbf{v}_e| + S_{\rm ph} \ , \tag{1a}$$

for positive ions,

$$\partial_t n_{\rm PI} = \alpha n_e |\mathbf{v}_e| + S_{\rm ph} \ , \tag{1b}$$

and for negative ions,

$$\partial_t n_{\rm NI} = \eta n_e |\mathbf{v}_e| \ , \tag{1c}$$

where n_e, $n_{\rm PI}$, and $n_{\rm NI}$ are the electron, positive-ion, and negative-ion densities, respectively, $\mathbf{v}_e$ is the average electron velocity, α is the electron-impact-ionization coefficient, η is the electron-attachment coefficient, and $S_{\rm ph}$ is the source of electron-ion pairs due to photoionization. The validity of these equations for the description of streamer dynamics has been discussed elsewhere.[17,18]

For the time scale of interest (longer than the electron energy relaxation time, but shorter than the characteristic time for ion motion), the electron current density can be obtained from the expression

$$n_e \mathbf{v}_e = -\mathsf{D}_e\cdot\nabla n_e - \mu_e n_e (\mathbf{E}_{\rm sp} + \mathbf{E}_a) \ , \tag{2}$$

where D_e is the diffusion tensor for electrons, μ_e is the electron mobility, and $\mathbf{E}_a$ and $\mathbf{E}_{\rm sp}$ are the applied and space-charge-induced field, respectively. The values used for the transport parameters (D_e and μ_e) and the rate coefficients (α, η, and $S_{\rm ph}$) in Eqs. (1) and (2) are those given by Wu and Kunhardt.[17] The space-charge field $\mathbf{E}_{\rm sp}$ follows from the solution of the Poisson equation

$$\nabla\cdot\mathbf{E}_{\rm sp} = \frac{q}{\epsilon}(n_{\rm PI} - n_e - n_{\rm NI}) \ , \tag{3}$$

where q is the charge, and ϵ is the dielectric constant of the gas. The numerical schemes for obtaining a solution to Eq. (1)–(3) have been extensively discussed in previous papers.[19–21]

B. Rate process formulation

To elucidate streamer dynamics from the viewpoint of process competition, we rewrite Eqs. (1a)–(1c) in the form of rate equations (at the point $\mathbf{r}$) and identify the various rate processes. Then, from Eqs. (1)–(3),

$$\frac{dn_e}{dt} = (-\nu_{\rm dft} + \nu_{\rm ER} + \nu_i^* + \nu_{s\,\rm sph}) n_e \ , \tag{4a}$$

$$\frac{dn_s}{dt} = \nu_{\rm dft} n_e - \nu_{\rm DR} n_s \ , \tag{4b}$$

where n_s is the total charge density ($n_{\rm PI} - n_e - n_{\rm NI}$), and the various rate coefficients are given by $\nu_i^* = (\alpha-\eta)|$, $\nu_{\rm DR} = n_e \mu_e q/\epsilon$, $\nu_{\rm ER} = n_s \mu_e q/\epsilon$, $\nu_{s\,\rm ph} = S_{\rm ph}/n_e$, and $\nu_{\rm dft} = -\mu_e \mathbf{E}\cdot\nabla(\ln n_e + \ln \mu_e)$, with $\mathbf{E} = \mathbf{E}_a + \mathbf{E}_{\rm sp}$. The contribution from the diffusion term has not been included in these equations since it is small compared to the other terms (this is discussed further below). Each of these rates can be identified with a physical process; namely, ν_i^* is the effective ionization rate, $\nu_{\rm DR}$ is the dielectric relaxation rate (the rate at which an excess charge at the point $\mathbf{r}$ decays with time), $\nu_{\rm ER}$ is the electron response rate due to the space charge (the rate at which an excess electron charge at the point $\mathbf{r}$ changes with time), $\nu_{s\,\rm ph}$ is the photoionization rate at $\mathbf{r}$, and $\nu_{\rm dft}$ is the drift rate (the rate at which the electron density at $\mathbf{r}$ changes with time due to drift in and out of a small volume about $\mathbf{r}$). From Eq. (4b), the $\nu_{\rm dft}$ term always tends to enhance the magnitude of the space-charge density, while the $\nu_{\rm DR}$ term tends to decrease it.

Similarly, a rate equation at the point $\mathbf{r}$ for the field can be obtained:

$$\frac{d\mathbf{E}}{dt} = \frac{\mathbf{J}'}{\epsilon} - \nu_{\rm DR}\mathbf{E} - \frac{q}{\epsilon}\mathsf{D}_e\cdot\nabla n_e \ , \tag{4c}$$

where $\mathbf{J}'$ is the total current density. From Eqs. (4a)–(4c), we can obtain relationships among the various rates which determine the "turning points" for n_e, n_s, and $\mathbf{E}$, that is, where the rate of change of these quantities changes sign or becomes zero.

These relations are presented in Sec. III in conjunction with the results obtained from numerical solutions of Eqs. (1)–(3).

III. RESULTS AND DISCUSSION

The results presented in this paper pertain to a cylindrically symmetric parallel-plate system with electrodes 0.5 cm apart, corresponding to 256 axial cells. The background gas density N is 2.45×10^{19} cm^{-3}. The transport parameters and rate coefficients used correspond to N_2 (nonattaching gas) and a 30–70 % mixture of SF_6-N_2 (attaching gas). The initial electron and ion distributions are equal and have the form of truncated Gaussian pulses located at the center of the space. That is,

$$n_e(t=0^+, r, z) = n_{\rm PI}(t=0^+, r, z) = 10^8 \exp\{-[r^2 + (z-0.25)^2]/(4.883\times10^{-3})^2\} \ \text{cm}^{-3} \ .$$

The space-charge field associated with this initial distribution is negligible compared to the applied field E_a. Because of this, and since the ionization rate is large for the situations of interest, the initial distribution has little effect on the final results. Unless stated otherwise, the applied field for the results presented is 82 kV/cm.

For these conditions, two-dimensional electron-density contours are shown in Figs. 1(a)–1(d) at various time steps, for the case $\eta = 0$; i.e., $\nu_i^* \equiv \nu_i \geq 0$. At $t = 0.65$ ns [Fig. 1(a)], the density of electrons is growing exponen-

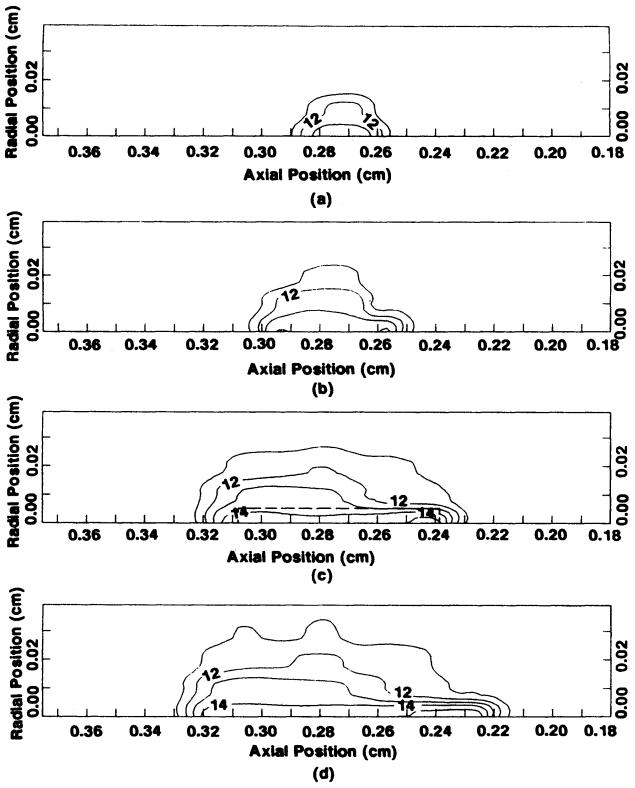

FIG. 1. Two-dimensional electron-density contour (ln scale) for times (a) 0.65 ns, (b) 0.79 ns, (c) 0.915 ns, and (d) 0.95 ns. The ratio between each contour line is 10:1 and the anode is located at 0.5 cm (the 256th cell). The dashed line in (c) defines the volume of integration discussed in Sec. III C.

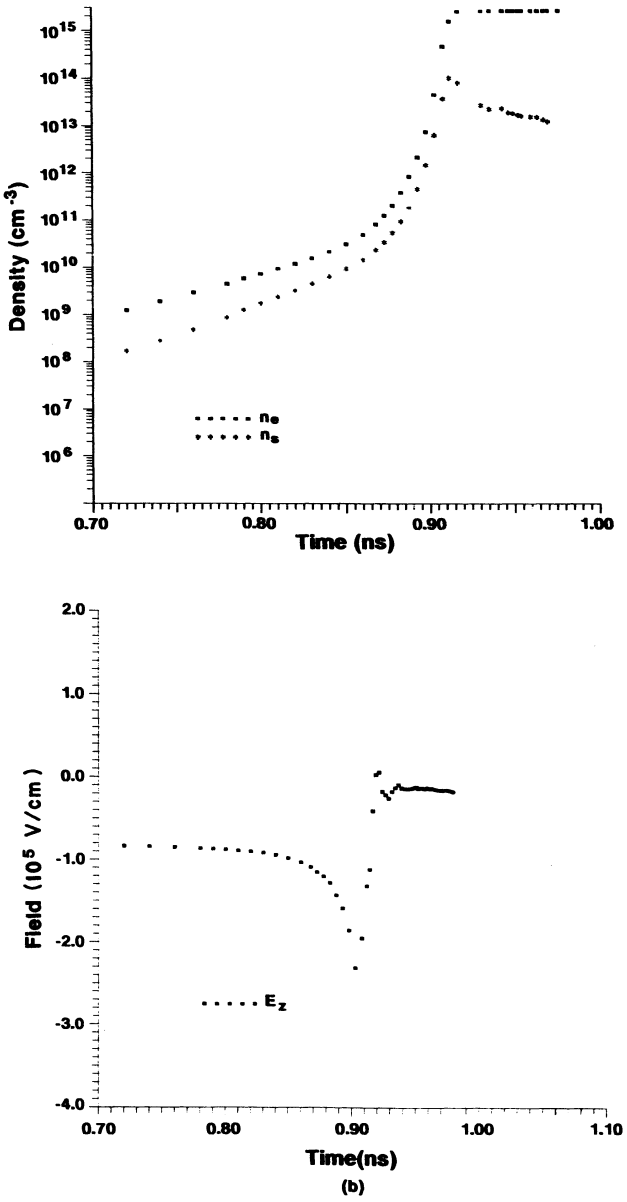

FIG. 2. (a) Time variation of the electron density (n_e) and space-charge density (n_s) at $z=0.2343$ cm corresponding to a CDS, (b) Time variation of the electric field (E) at the same position.

tially. Subsequently [Figs. 1(b)–1(d)] the anode-directed streamer (ADS) forms, followed shortly by the cathode-directed streamer (CDS). The general features of these streamers have been previously discussed.[17] From Figs. 1(c) and 1(d), electron density for the ADS front "saturates" at approximately 10^{14} cm^3, while for the CDS at 10^{15} cm^{-3}. Moreover, the CDS is radially narrower than the ADS. Insight into the dynamical characteristics of the steamer fronts can be obtained by looking at the temporal evolution of the electron density, space-charge density, and electric field at a fixed position. In Figs. 2(a) and 2(b), these quantities are plotted for the axial cell at $z=0.2343$ cm (cathode side of the initial distribution). As shown in Fig. 2(a), the electron density grows exponentially up to $t=0.9025$ ns, after which the growth rate decreases monotonically until the density saturates at $t=0.915$ ns. The behavior of the space-charge density n_s is very similar up to $t=0.915$ ns, at which point it reaches a maximum (i.e., turning point), and subsequently decays until eventually it becomes negligible (the temporal and spatial behavior of the particle densities are correlated; this is discussed further below). Similarly, the total electric field increases with time up to $t=0.9025$ ns, due to the increase in the space-charge field; subsequently, it decreases with time and overshoots (at $t=0.93$ ns) its final value in the body of the streamer. This value is much less than that of the applied field.

From these observations, and using Eqs. 4(a)–4(c), we identify five stages or domains of evolution. (I) Preionization domain, where $\nu_{s\,\mathrm{ph}} > \nu_i > \nu_{\mathrm{dft}}$. In this regime, the electron density at the point r is determined by photoionization. In effect, the density in this regime is a stochastic function of position. However, because of subsequent ionization growth of each of these "seed" electrons, the influence of the space-charge field, and diffusion, the initial statistical fluctuations in density are smoothed out. Thus, in the next and subsequent stages, the particle densities are well described by their average values. This is

substantiated by Monte Carlo simulations.[18] Consequently, the corresponding average densities are also used in the photoionization domain. (II) Ionization domain, where $d\nu_i/dt>0$ and $\nu_i>\nu_{\rm dft}>\nu_{\rm DR}>|\nu_{\rm ER}|$. In this regime, the dominance of the ionization rate term in Eq. 4(a) results in an exponential growth in electron density. Initially, the growth rate increases with the space-charge density and field. However, as the electron density increases, the conductivity increases, allowing electron "currents" to flow that tend to decrease the space-charge field and thus the ionization rate. This initiates the third (III) regime, the conductivity domain, where $d\nu_i/dt<0$ and $\nu_{\rm DR}\approx\nu_i>\nu_{\rm dft}\gtrsim|\nu_{\rm ER}|$. Although the ionization rate decreases with time in this stage, the electron density continues to increase (but no longer exponentially) and eventually $\nu_{\rm DR}>\nu_i>|\nu_{\rm ER}|\simeq\nu_{\rm dft}$. At this time, the space-charge density reaches a maximum which is used to define the fourth stage (IV), the maximum n_s domain. Finally, the dielectric relaxation rate dominates over all other processes ($\nu_{\rm DR}\gg|\nu_{\rm ER}|>\nu_i$) and the electron density saturates [(V) electron-density saturation domain]. This occurs for

$$n_e=n_e(-\nu_{\rm dft}+\nu_i+\nu_{s\,\rm ph})/\nu_{\rm DR}+n_{\rm PI}\ , \tag{5}$$

and since $\nu_{\rm DR}\gg\nu_i$, $\nu_{\rm dft}$, and $\nu_{s\,\rm ph}$; $n_e\simeq n_{\rm PI}$. From Eq. 4(c), the rate of change of space-charge-field enhancement, $d|\mathbf{E}|/dt$, becomes negative at large n_e, i.e., large $\nu_{\rm DR}$. Physically, this corresponds to the transformation of displacement current into convection current. Thus, to reach the saturation domain (stage V) at point **r**, the following events occur sequentially: (1) increase in n_e leads to a reduction in **E** and consequently ν_i and $\nu_{\rm dft}$; (2) the space-charge-density peak moves across the cell at **r**; and (3) dielectric relaxation, $\nu_{\rm dr}\gg\nu_i$, leads to a saturation in n_e. This sequence is further discussed in the following subsections.

A. Electric density saturation: $\eta=0$ and $\nu_i^*=\nu_i$

1. Temporal analysis

Consider the temporal behavior of the electron density at a fixed spatial cell due to the passage of the streamer front [see Figs. 2(a) and 2(b)]. The corresponding variation in time of the various rates appearing in Eq. (4) are shown in Figs. 3(a) and 3(b). For CDS and times less than 0.83 ns, the observing cell is far away from the streamer front so that the electron density and the space-charge field are negligible. The ionization rate is solely determined by the constant applied field. From 0.83 to 0.9025 ns (ionization domain), the ionization rate increases due to the enhancement of the field by the approaching streamer front with a concomitant enhanced avalanche growth of the electron density. A density is reached for which electron conductivity is significant and $d\nu_i/dt<0$. In this stage, n_s increases rapidly since it depends on $\nu_{\rm dft}$ ($\approx v_e\cdot\nabla(\ln(n_e))\propto|v_e|\alpha(E)\approx\nu_i$), which increases with n_e. From 0.9025 to 0.91 ns (conductivity domain), the space-charge field decreases, reducing the ionization rate and the growth of the electron density. ν_i

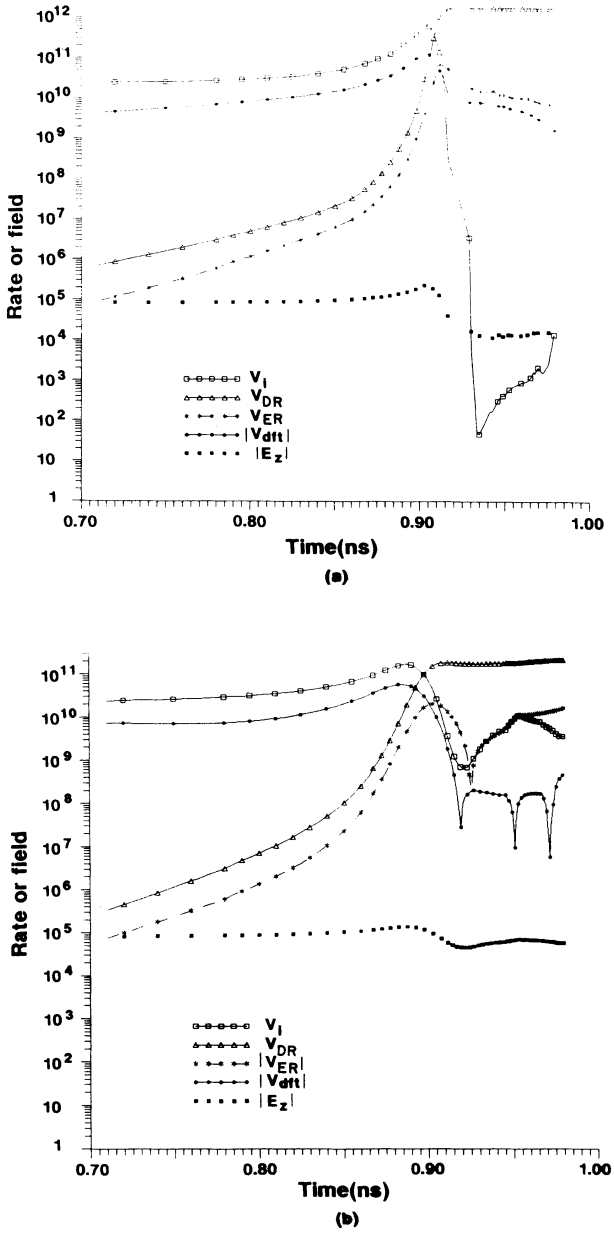

FIG. 3. (a) Time variation of various rates and E field on CDS at the same position as in Fig. 2. (b) Time variation of various rates and E field at $z=0.3066$ cm corresponding to an ADS.

becomes comparable to $\nu_{\rm DR}$. At the same time, the growth rate of n_s becomes smaller due to the increase in $\nu_{\rm DR}$ and the decrease in $\nu_{\rm dft}$. From 0.91 to 0.915 ns (peak n_s domain), n_s reaches its peak value and begins to decay due to the balancing between $\nu_{\rm dft}$ and $\nu_{\rm ER}$. The peak n_s manifests itself as a global temporal constant since both $\nu_{\rm dft}$ and $\nu_{\rm ER}$ are slowly varying functions of time in this domain. Physically, the temporal evolution of n_s images its spatial propagation with the peak n_s as the space-charge center. Subsequently, the total E field at the observing cell decreases as the space-charge field reverses

direction due to the passage of the center of the space charge. The peak n_s behaves like a constant of the motion for either CDS or ADS. Any disturbance results in a stronger space-charge field, which leads to an exponential increase in ν_i and n_e. The temporal saturation of n_e implies that ν_{ER} and ν_{dft} always balance at the same n_s, and that the E field and the electron-density gradient in this domain are constants in time. At 0.915 ns (saturation domain), ν_{ER} becomes comparable to ν_i and both have negligible second-order effect on n_e, resulting in the saturation of n_e. After 0.915 ns, both the electron density and the positive-ion density are temporally frozen because all pertinent rates (ν_i and ν_{ER}) continue to decrease. The behavior of the density for an observing cell at $z=0.3066$ cm on the side of ADS is shown in Fig. 3(b). The dynamics are similar to that indicated above.

2. *Spatial analysis*

The spatial characteristics of streamers are shown in Fig. 4 at times 0.79 ns [Fig. 4(a)] and 0.915 ns [Fig. 4(b)]. These times correspond to partial and completely formed streamers, respectively. Generally speaking, the spatial characteristics image the temporal characteristics. That is, we may interchange the role of space and time since the characteristics of the streamer front are (nearly) stationary in a frame moving at its phase velocity v_{ph}. Thus each temporal stage corresponds to a spatial section (domain) of the streamer front. As seen from Fig. 4(b), inside the conductivity domain (in the axial range 0.231–0.234 cm for CDS and 0.308–0.312 cm for ADS), the large density of mobile electrons is able to shield partially the applied field and reduce the accumulation rate of space charge. Note that the peak electron density at this time is located near the boundary between the conductivity and saturation domains. This implies that the peak electron density is near the upper bound set by the saturation density. Thus the streamer bulk behind the peak electron density is stabilized. Thus represents a spatial saturation effect. In the ionization domain (in the axial range 0.23–0.211 cm for CDS and after 0.31 cm for ADS), the electron and ion densities increase until they reach the conductivity domain. During the time of enhanced ionization, the charge separation induced by the drift term creates a propagating space-charge center. In the preionization domain (for axial positions less than 0.211 cm for CDS), most of the electron-ion pairs are generated by photoionization as opposed to impact ionization. As can be observed, the photoionization term for ADS is not as important as for CDS. The reasons for this influence on the CDS are the following: (1) The photoionization rate is proportional to the nearby distributed ionization process, which is stronger for CDS, and (2) the drift term is able to provide electrons in front of ADS which immediately grow due to ionization; this is not so for the CDS. Note that the enhanced ν_i for CDS is larger than that of the ADS. (The reason for this difference in ν_i is explained in the next section.) This causes the saturation density in CDS to be one order of magnitude higher than that in ADS. In fact, for a constant applied voltage there is a slow spatial increase in

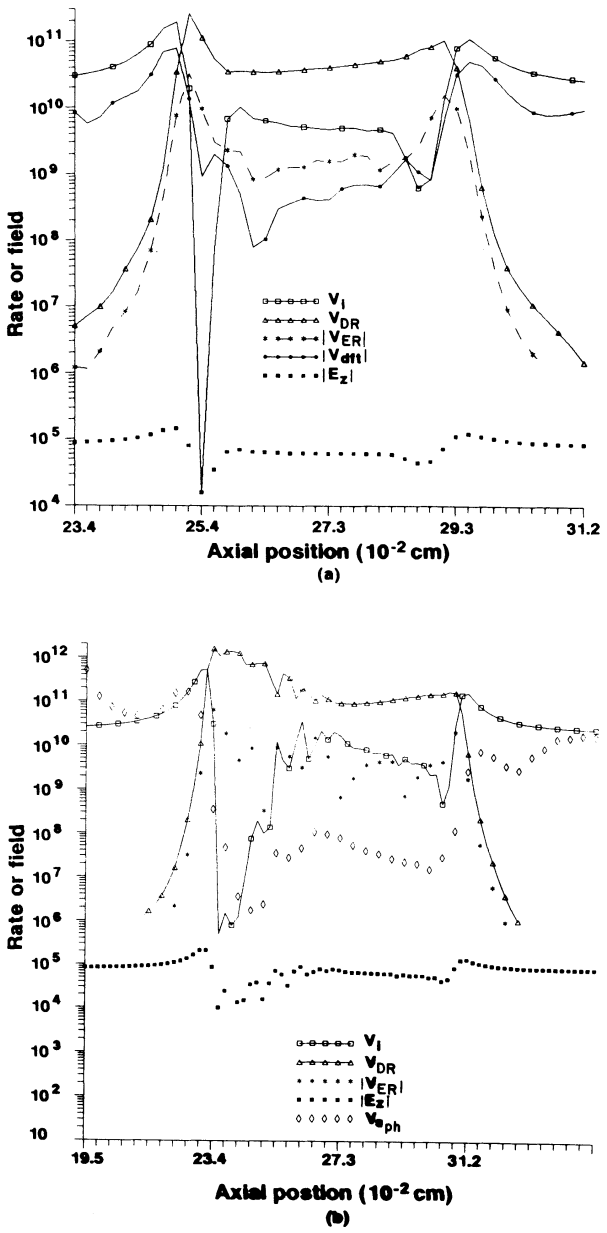

FIG. 4. (a) Spatial variation of the various rates and E field at 0.79 ns corresponding to Fig. 1(b). (b) Spatial variation of the various rates and E Field at 0.915 ns corresponding to Fig. 1(c).

electron density in front of the streamer. This spatial variation results from a "potential compensation" effect; i.e., the E field is enhanced in front of streamer to compensate for the potential loss in the streamer bulk. As both streamers propagate, the length of the streamer body increases so that the field in front of the streamer fronts increase to "compensate" the "losses" in the bulk. Thus the "effective" field seen by the propagating streamer increases with propagation distance. In a real situation, there is an internal resistance associated with the power supply. Thus, as the conductivity increases in the streamer bulk, the current flowing through the internal

resistor will increase such that the potential loss in the streamer bulk is compensated by a potential increase in the internal resistor, making possible the steady-state propagation of the streamer fronts. A small oscillation in n_s (compared to n_e) appears when the reverse space-charge field is much stronger than applied field, as in Fig. 4(b). This causes ν_i to oscillate. This overshoot of the space-charge field is responsible for the appearance of secondary streamers.[15,17] It is shown in Fig. 2(a) that this oscillation is more important in CDS due to its stronger space-charge-field distortion as discussed below.

We can summarize the spatiotemporal streamer dynamics as follows. First, photoionization generates the initial electron which starts the impact-ionization mechanism. Second, ionization leads to the avalanche growth of the positive-ion–electron densities and builds up the steep streamer front, which gives rise to a significant drift rate term. Third, the drift-rate term builds up a new space-charge center, while the dielectric relaxation term removes the previous one at the previous cell. The advancement of the space-charge center reduces the total field and saturates n_e. The combined effect is a propagating space-charge center and an extending streamer body. The ordering of the characteristic domains corresponds to the dominant mechanism during that phase of evolution.

B. Fundamental differences between CDS and ADS

From the simulation results we have found three major differences between CDS and ADS: (1) the saturated n_e at CDS is one order of magnitude larger than that at ADS, (2) the phase velocity of CDS is about twice that of ADS, and, (3) the saturated n_e at CDS increases slowly in space with a pronounced oscillating component. These differences are primarily a consequence of (a) the direction of particle flow due to radial diffusion with respect to their drift and (b) the effectiveness of the electron flow in modifying the local space-charge field. Consider this last point in the context of a fixed cell in the ionization domain. For CDS, electrons from this cell are continuously transported by the drift term into the conductivity domain where they constitute a small percentage of the total density. Thus these electrons only contribute to the further decrease of the already small E field in this region (recall that ionization in this region is small). On the other hand, electrons at the ADS are transported forward into a region of lower density, thus significantly contributing to the decrease of the enhanced E field and, correspondingly, the growth rate in the ionization domain.

With regard to the direction of particle flow in the streamers, the radial diffusion inside the saturation domain of the CDS is canceled by the radial drift alone, so that ionization is not required to participate in the balancing. To the contrary, for the ADS, both radial drift and diffusion are directed outwards. Therefore, a substantial ionization rate (or axial electric field) is required to compensate this radial loss and maintain the radial profile. Accordingly, ν_i for the CDS is smaller in both the conductivity and saturation domains, and larger in the ionization domain due to the potential compensation effect. Because the ionization domain is the period during which the electron density is exponentially increasing, the accumulation time for the CDS required to reach the saturated density is thus smaller, which implies a larger $v_{\rm ph}$. The observed oscillation increase in the saturated n_e for the CDS is due to the stronger space-charge-field distortion required to acquire a higher field in the ionization domain and a lower field in the saturation domain.

C. Correlation between CDS and ADS

From the discussion in Sec. III, it is evident that the electron density in the streamer front reaches its saturated value as result of competition between ionization and dielectric relaxation. This saturated electron density is an implicit function of the gas parameters and the applied field, but not of the initial electron density. The issue that needs to be addressed is how to explicitly evaluate or predict this saturated density. This is a difficult task since the dynamics of the front is strongly nonlinear. However, we have been able to obtain a relation between the electron densities in both streamers. To achieve this, integrate $\nabla\cdot\mathbf{J}'=0$ in a volume bounded by a closed surface defined by the boundary between the conductivity and saturation domains of both streamers, where $d(\mathbf{E})/dt$ is zero, and the boundary of the first cell on the z axis. An example of such a closed surface is shown in Fig. 1(c). Neglecting the axial diffusion current, we have

$$(n_e\mathbf{E}|_{\rm CDS}-n_e\mathbf{E}|_{\rm ADS})\mu_e\pi r^2 = 2\pi r\Delta L_{\rm ADS}\left[D_t\frac{\partial n_e}{\partial r}+\mu_e E_r n_e\right], \quad (6)$$

where the subscripts inside the parenthesis on the left-hand side indicate the evaluation of the product at the

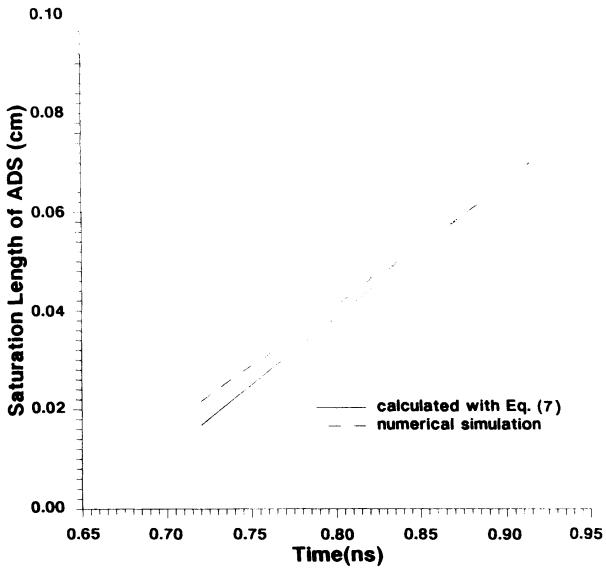

FIG. 5. Saturation length of ADS.

corresponding boundary, r is the radius of the first cell on the z axis, and $\Delta L_{\rm ADS}$ is the spatial length of the saturation domain of the ADS.

Because the radial convection current is balanced by ionization in the first cell (in order to maintain the electron density in the ADS), the right-hand side of Eq. (6) can be replaced by $\pi r^2 \Delta L_{\rm ADS}(\nu_i n_e)$, resulting in the expression

$$(n_e E|_{\rm CDS} - n_e E|_{\rm ADS})\mu_e = \Delta L_{\rm ADS}(\nu_i n_e)|_{\rm ADS} . \quad (7)$$

As previously established, $n_e E|_{\rm CDS}$ has a minimum determined by the potential compensation effect. Thus a minimum $\Delta L_{\rm ADS}$ is required to start the CDS propagation. That is, the ADS always starts first. In Fig. 5 we have plotted the saturation length $\Delta L_{\rm ADS}$ obtained from Eq. (7) and directly from the simulation results. The consistency between these results is satisfactory.

D. Velocity of streamer front

From the definition of the drift rate $\nu_{\rm dft}$, an expansion can be developed at the boundary between the peak n_e and the saturation point where the streamer front has a phase velocity $v_{\rm ph}$. That is,

$$\nu_{\rm dft} = -\mu e \mathbf{E}\cdot\nabla \left[[\ln n_e(t_0)] + \int_{t_0}^{t} (\nu_i - \nu_{\rm dft})(\tau) d\tau \right]$$

$$= \frac{v_e}{-v_{\rm ph}} (\nu_i - \nu_{\rm dft}) , \quad (8a)$$

or

$$\frac{v_{\rm ph}}{v_e} = \frac{\nu_i - \nu_{\rm dft}}{-\nu_{\rm dft}} . \quad (8b)$$

We have also calculated the streamer phase velocity computationally. Since $v_{\rm ph}$ is the velocity along the axis of a point of constant density, we obtain, from Eq. (1a),

$$v_{\rm ph} = u_z + \frac{n_e(\partial_z u_z - \alpha|u_z| - S_{\rm ph})}{\partial_z n_e} , \quad (9)$$

where u_z is the axial component of $\mathbf{u}_e$. A more accurate result for $v_{\rm ph}$ [which takes into account higher-order terms than those in Eq. (9)] is obtained by computing $\Delta z/\Delta t$ for a point on the front at a fixed density. In Fig. 6 we have plotted for comparison the computed $\Delta z/\Delta t$, calculated [Eq. (9)], and the theoretical [Eq. (8b)] phase velocity for both directed streamers. The values estimated by Eq. (8b) are quite consistent with other results.

E. Electron-density saturation: $\eta \neq 0$

The primary difference between nonattaching and attaching gases is that electrons inside the conductivity domain are fast immobilized in the latter case and lose their abilities to shield out the applied field.[15,16] As a result, the reduced local field inside the conductivity domain bounces back to a value above that in a nonattaching gas. A steady-state electron density can only be achieved if the E field inside the streamer bulk is maintained just above the critical field ($E_{\rm cr}$), defined by $\alpha^*(E_{\rm cr}) = \alpha - \eta = 0$. For $|E_{\rm cr}| = 6.8027 \times 10^4$ V/cm in our simulation, $\nu_i^*(E_{\rm cr})$ equals 8.8 GHz, which is just below ν_i^* in the streamer bulk. If $E_{\rm cr}$ is higher than the field required to balance the radial current outflow, the saturation electron density in the ADS is larger than that associated with the balance field; moreover, the spatial oscillations in density are significantly larger.[17] This assertion is verified by Fig. 7.

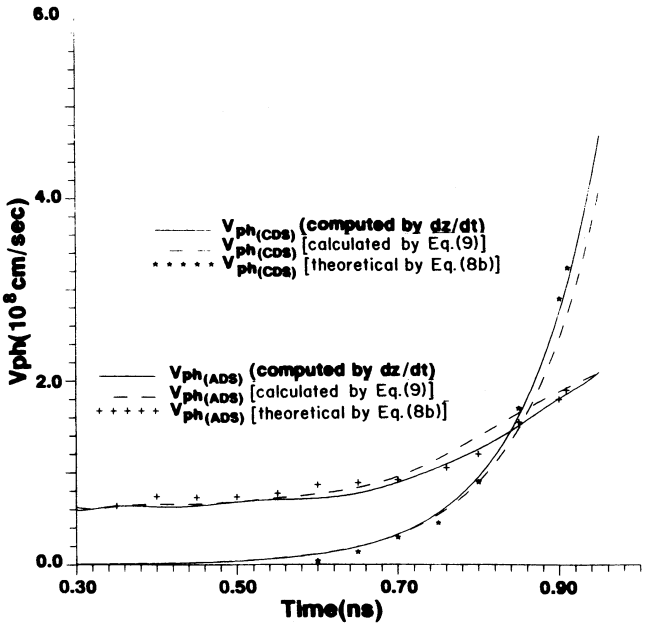

FIG. 6. Time variation of $v_{\rm ph}$.

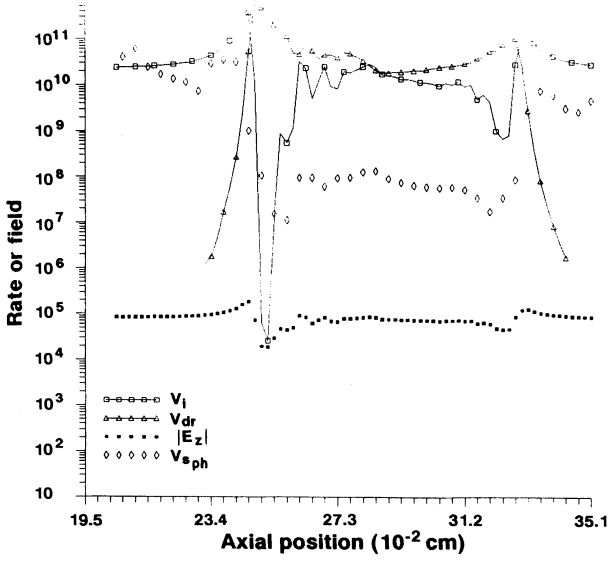

FIG. 7. Spatial variation of the various rates and E field at 1.4 ns (attaching gas).

IV. CONCLUDING REMARKS

In this paper we have analyzed streamer dynamics from the viewpoint of process competition. It has been found that the steady-state streamer is established by the detailed balancing of those competing processes. In particular, the displacement of the streamer front along the field direction is due to the generation of a new maximum in space-charge density by the drift rate at a location adjacent to the previous maximum and the removal of the previous maximum by dielectric relaxation. The origin of the differences between the CDS and ADS has been identified with (a) the direction of electron flow due to radial diffusion with respect to radial drift (for CDS, the flows are antiparallel, whereas for ADS, they are parallel and outward from the center), and (b) the effectiveness of the electron flow in modifying the local space-charge field (for CDS, the flow has little effect on the field in the ionization region, whereas for ADS, it tends to decrease it significantly). From the relation between the CDS and ADS fronts, we have determined that the ADS forms first and that the formation of the ADS requires a minimum length of CDS propagation.

ACKNOWLEDGMENTS

This work has been supported by the Office of Naval Research.

[1]L. B. Loeb, Science **148**, 1417 (1965).
[2]G. A. Dawson and W. P. Winn, Z. Phys. **183**, 159 (1965).
[3]R. Klingbeil, D. A. Tidman, and R. F. Fernsler, Phys. Fluids **15**, 1969 (1972).
[4]R. G. Fowler, Adv. Electron. and Electron Phys. **41**, 1 (1976).
[5]R. F. Fernsler, Phys. Fluids **27**, 1005 (1984).
[6]I. Gallimberti, J. Phys. (Paris) **40**, 193 (1979).
[7]L. B. Loeb, in *Handbook of Physics,* edited by S. Flugge (Springer-Verlag, Berlin, 1956), Vol. 22, p. 445.
[8]K. H. Wagner, Z. Phys. **189**, 465 (1966).
[9]P. Stritzke, I. Sanders, and H. Raether, J. Phys. D **10**, 2285 (1982).
[10]W. W. Byszewski, J. J. Enright, and J. M. Proud, IEEE Trans. Plasma Sci. **PS-10**, 281 (1982).
[11]W. Pfeigger, A. Leit, P. Volker, and H. Fischer, Appl. Opt. **20**, 10 (1981).
[12]P. F. Williams and F. E. Peterkin, J. Appl. Phys. **66**, 4163 (1989).
[13]L. E. Kline and J. Siambis, Phys. Rev. A **5**, 794 (1972).
[14]K. Yoshida and H. Tagashira, J. Phys. D **9**, 485 (1976).
[15]S. Dhali and P. F. Williams, Phys. Rev. A **31**, 1219 (1985).
[16]R. Morrow, Phys. Rev. A **35**, 1778 (1987).
[17]C. Wu and E. E. Kunhardt, Phys. Rev. A **37**, 4396 (1988).
[18]E. E. Kunhardt and Y. Tzeng, Phys. Rev. A **38**, 1410 (1988).
[19]E. E. Kunhardt and P. F. Williams, J. Comput. Phys. **57**, 403 (1985).
[20]C. Wu and E. E. Kunhardt, J. Comput. Phys. **84**, 247 (1989).
[21]E. E. Kunhardt and C. Wu, J. Comput. Phys. **68**, 127 (1987).